Synchronization at Startup and Stable Rotation Reversal of Sensorless Nonsalient PMSM Drives

Magnus Jansson, Lennart Harnefors, *Member, IEEE*, Oskar Wallmark, *Student Member, IEEE*, and Mats Leksell, *Member, IEEE*

***Abstract*—In this paper, a variant of the well-known "voltage model" is applied to rotor position estimation for sensorless control of nonsalient permanent-magnet synchronous motors (PMSMs). Particular focus is on a low-speed operation. It is shown that a guaranteed synchronization from any initial rotor position and stable reversal of rotation can be accomplished, in both cases under load. Stable rotation reversal is accomplished by making the estimator insensitive to the stator resistance. It is also shown that the closed-loop speed dynamics are similar to those of a sensored drive for speeds above approximately 0.1 per unit, provided that the model stator inductance is underestimated. Experimental results support the theory.**

***Index Terms*—Permanent-magnet synchronous motor (PMSM), position estimation, sensorless control, stability analysis.**

I. Introduction

SENSORLESS salient permanent-magnet synchronous motors (PMSMs)—having rotors with buried or inset magnets—can utilize signal-injection methods [1], [2] for estimation of the rotor position. Signal-injection methods give an accurate rotor position estimate at all speeds. Recent enhancements have allowed injection methods to be used also for motors with small saliency (here, for simplicity, called nonsalient motors), i.e., PMSMs with surface-mounted magnets [3], [4]. However, a fairly complex algorithm appears to be required in order to mitigate problems such as a nonsinusoidal impedance distribution and nonlinear inverter effects. Another drawback is that signal injection, at least to some extent, causes extra losses and torque ripple.

Position estimation methods based on the back electromotive force (EMF)—so-called back-EMF-based methods[1]—generally give good performance at nominal and high speeds. Because the back EMF is proportional to the speed, any back-EMF-based sensorless scheme becomes "blind" at zero speed. Convergence of the estimated rotor position to the actual position then cannot be guaranteed. As a consequence, three instability phenomena commonly occur at low speeds.

1) Initial rotation in the wrong direction. Since the rotor position is unknown, 50% (statistically) of the times the motor is started, it initially rotates "backwards." This cannot be prevented, but the "backward" rotation should be reversed as quickly as possible.
2) Synchronization failure, giving lockup at a low speed. At startup, the estimated position may fail to converge to the actual position, resulting in lockup at a low speed (with an erroneous sign). This may occur also for rotation reversals.
3) Limit cycles. A sustained oscillation about a low speed can appear when the rotation is about to reverse. This is a problem mainly for reversal under load.

Reliable start and synchronization from standstill can be achieved simply by a proper current and a frequency control, without any rotor position feedback. The stator frequency is gradually increased, until it is sufficiently high for the position estimator to be phased in safely; e.g., [5]. This method, however, requires that the load torque is low during the startup process.

Proposals for closed-loop sensorless systems that give reliable start and rotation reversal under load are relatively rare. In [6], it is shown that, for the algorithm in [7], synchronization is not guaranteed, but can be, if the algorithm is modified. In [8], a countermeasure against rotation in the wrong direction is added to an extended-Kalman-filter-type algorithm. The algorithms in [9], [10] are experimentally shown to give guaranteed synchronization, although no strict proof thereof is presented.

In this paper, after setting the stage in Section II, we, in Section III, analyze and further develop low-speed properties of the position estimator developed and evaluated in [11] and [12]. This estimator is a variant of the well-known "voltage model." The contribution is the prevention of the aforementioned low-speed instability phenomena.

1) Guaranteed synchronization at startup—even after brief transient "backward" rotation—is established in a more rigorous way than in [11], by a combination of analysis and multiple simulations. In this process, selection recommendations for the estimator's gain parameters are derived.

Manuscript received June 28, 2004; revised January 22, 2005. Abstract was published on the Internet January 25, 2006.

M. Jansson was with the Department of Electronics, Mälardalen University, SE-721 23 Västerås, Sweden. He is now with ABB Automation Products, SE-721 70 Västerås, Sweden (e-mail: magnus.x.jansson@se.abb.com).

L. Harnefors was with the Department of Electronics, Mälardalen University, SE-721 23 Västerås, Sweden. He is now with ABB Power Systems, SE-771 80 Ludvika, Sweden (e-mail: lennart.harnefors@se.abb.com).

O. Wallmark is with the Department of Energy and Environment, Chalmers University of Technology, SE-412 96 Göteborg, Sweden (e-mail: oskar.wallmark@chalmers.se).

M. Leksell is with the School of Electrical Engineering, Royal Institute of Technology, SE-100 44 Stockholm, Sweden (e-mail: mats.leksell@ets.kth.se).

Digital Object Identifier 10.1109/TIE.2006.870731

[1]Not to be confused with back-EMF-sensing methods for sensorless control of brushless dc motors.

2) An accurate estimate of the stator resistance is, normally, critical for a good performance at low speeds. The sensitivity to the stator resistance is here eliminated by using $i_d \neq 0$ (but keeping $|i_d|$ relatively small; $|i_d| \leq |i_q|/2$). This enables rotation reversal even under load.

In addition, good dynamics for closed-loop speed control, when the model stator inductance is underestimated, are demonstrated analytically in Section III, and experimental results verifying the theory are presented in Section IV.

As can be seen in Appendix C, the proposed estimator is quite simple to implement on a digital signal processor (DSP); in fact, simpler than the aforementioned current and frequency control starting method. While a specific position estimator is considered, the analysis method is general, and should be applicable also to other candidate estimators.

II. Model and Estimator

In the synchronous (dq) reference frame, the dynamic electrical model for the nonsalient PMSM is given by [11]

$$\mathbf{v}_\mathrm{s} = \underbrace{L_\mathrm{s}\frac{d\mathbf{i}_\mathrm{s}}{dt}}_{\approx 0} + (R_\mathrm{s} + j\omega_1 L_\mathrm{s})\mathbf{i}_\mathrm{s} + j\omega_\mathrm{r}\psi_\mathrm{m}e^{j\tilde{\theta}} \tag{1}$$

where $\mathbf{v}_\mathrm{s} = v_d + jv_q$ is the applied stator voltage vector, $\mathbf{i}_\mathrm{s} = i_d + ji_q$ is the stator current vector, ψ_m is the permanent-magnet flux linkage modulus, L_s the stator inductance (which is assumed constant, i.e., not a function of the rotor position), and R_s is the stator resistance, respectively. As in [11], fast and accurate closed-loop current control is assumed, such that $\mathbf{i}_\mathrm{s} = \mathbf{i}_\mathrm{s}^\mathrm{ref} = i_d^\mathrm{ref} + ji_q^\mathrm{ref}$ (where superscript "ref" denotes reference to the current controller), allowing $L_\mathrm{s}(d\mathbf{i}_\mathrm{s}/dt)$ to be neglected—as indicated in (1)—seen from the slower dynamics of the position estimator.

Observe that the dq frame is that "seen" by the control system; it is displaced from the stationary $(\alpha\beta)$ frame by the estimated rotor position $\hat{\theta}$. This dq frame does not generally coincide with that of the motor, which is displaced by the true rotor position θ. Hence, the appearance of the transformation factor $e^{j\tilde{\theta}}$ in the back EMF $j\omega_\mathrm{r}\psi_\mathrm{m}e^{j\tilde{\theta}}$, where $\tilde{\theta} = \theta - \hat{\theta}$. The electrical torque is, thus, proportional to $\mathrm{Re}\{\mathbf{i}_\mathrm{s}e^{j\tilde{\theta}}\} = i_q\cos\tilde{\theta} - i_d\sin\tilde{\theta}$, which reduces to the ideal i_q for $\tilde{\theta} = 0$. Finally, $\omega_\mathrm{r} = \dot{\theta}$ and $\omega_1 = \dot{\hat{\theta}}$, giving

$$\dot{\tilde{\theta}} = \omega_\mathrm{r} - \omega_1. \tag{2}$$

The back EMF contains speed and position-error information, though not independent of each other [11]. An estimate of the back EMF can be obtained by subtracting the resistive and inductive voltage drops from (1)

$$\mathbf{e} = \mathbf{v}_\mathrm{s} - (\hat{R}_\mathrm{s} + j\omega_1\hat{L}_\mathrm{s})\mathbf{i}_\mathrm{s}^\mathrm{ref} \tag{3}$$

or, in component form, with $\mathbf{e} = e_d + je_q$

$$e_d = v_d - \hat{R}_\mathrm{s}i_d^\mathrm{ref} + \omega_1\hat{L}_\mathrm{s}i_q^\mathrm{ref} \tag{4}$$

$$e_q = v_q - \hat{R}_\mathrm{s}i_q^\mathrm{ref} - \omega_1\hat{L}_\mathrm{s}i_d^\mathrm{ref} \tag{5}$$

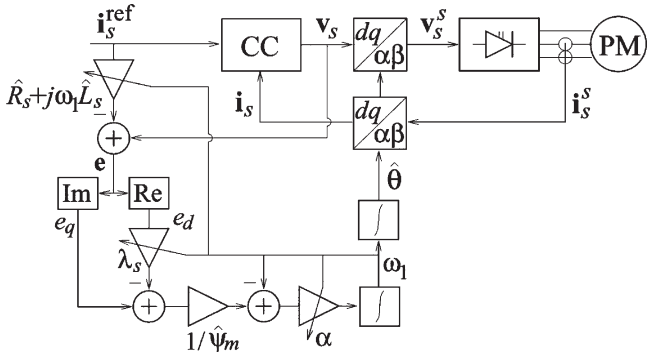

Fig. 1. Sensorless vector control system, where "CC" is the current controller, $\lambda_\mathrm{s} = \lambda\mathrm{sgn}(\omega_1)$, and $\alpha = \alpha_0 + 2\lambda|\omega_1|$.

where $\hat{R}_\mathrm{s}$ and $\hat{L}_\mathrm{s}$ are the model stator resistance and stator inductance, respectively.

The "statically compensated voltage model" of [11] is adopted as position estimator

$$\dot{\omega}_1 = \alpha\left(\frac{e_q - \lambda_\mathrm{s}e_d}{\hat{\psi}_\mathrm{m}} - \omega_1\right) \qquad \dot{\hat{\theta}} = \omega_1 \tag{6}$$

where $\hat{\psi}_\mathrm{m}$ is a static estimate [1 per unit (pu)] of the permanent-magnet flux linkage modulus and $\lambda_\mathrm{s} = \lambda\mathrm{sgn}(\omega_1)$, where $\mathrm{sgn}(\cdot)$ is the sign function. The positive gains λ and α (the latter being the bandwidth of the low-pass filter in which the selection of ω_1 is embedded) are selected in the next section. A block diagram of the sensorless vector control system is depicted in Fig. 1. Notice that the estimator can utilize the output voltage vector of the current controller, which, after $\alpha\beta$ transformation, serves as reference for the pulsewidth modulator of the inverter. Measurement of the stator voltage is thereby avoided. A sample C-code implementation is presented in Appendix C.

III. Analysis

In this section, we analyze the properties of the estimator, with the goal of avoiding the instability phenomena discussed in the Introduction. In this process, useful selection rules for the estimator's gain parameters as well as the model motor parameters are obtained. To allow analysis of the dynamics as well as the impact of erroneous model motor parameters, the real and imaginary parts of the right-hand side of (1) are substituted for v_d and v_q in (4) and (5)

$$e_d = \underbrace{\tilde{R}_\mathrm{s}i_d - \omega_1\tilde{L}_\mathrm{s}i_q}_{\tilde{e}_d} - \omega_\mathrm{r}\psi_\mathrm{m}\sin\tilde{\theta} \tag{7}$$

$$e_q = \underbrace{\tilde{R}_\mathrm{s}i_q + \omega_1\tilde{L}_\mathrm{s}i_d}_{\tilde{e}_q} + \omega_\mathrm{r}\psi_\mathrm{m}\cos\tilde{\theta} \tag{8}$$

where $\tilde{R}_\mathrm{s} = R_\mathrm{s} - \hat{R}_\mathrm{s}$ and $\tilde{L}_\mathrm{s} = L_\mathrm{s} - \hat{L}_\mathrm{s}$. Substituting (7) and (8) in (6), we obtain

$$\dot{\omega}_1 = \alpha\left(\frac{\tilde{e}_q + \omega_\mathrm{r}\psi_\mathrm{m}\cos\tilde{\theta} - \lambda_\mathrm{s}(\tilde{e}_d - \omega_\mathrm{r}\psi_\mathrm{m}\sin\tilde{\theta})}{\hat{\psi}_\mathrm{m}} - \omega_1\right). \tag{9}$$

This fundamental relation—which includes all parameters critical for the dynamic and steady-state performance of the sensorless control system—together with the position-error dynamics (2) form the nonlinear second-order system that will be analyzed in the following.

A. Selection of Gain Parameters for Synchronized Operation

Suppose for the moment that $\tilde{e}_d = \tilde{e}_q = 0$, $\hat{\psi}_{\rm m} = \psi_{\rm m}$, and $\tilde{\theta}$ is small, such that $\cos\tilde{\theta} \approx 1$ and $\sin\tilde{\theta} \approx \tilde{\theta}$. Then, (9) simplifies to

$$\dot{\omega}_1 = \alpha(\omega_{\rm r} - \omega_1 + \lambda_{\rm s}\omega_{\rm r}\tilde{\theta}) \tag{10}$$

so as long as $\lambda_{\rm s}\omega_{\rm r} > 0$, positive feedback of both the speed error $\omega_{\rm r} - \omega_1$ and the position error $\tilde{\theta} = \theta - \hat{\theta}$ is provided. Assuming a slowly varying rotor speed: $\dot{\omega}_{\rm r} \approx 0$, and introducing $\tilde{\omega} = \omega_{\rm r} - \omega_1$ (which is assumed small), (10) and (2) together form the following linearized second-order system

$$\dot{\tilde{\omega}} = -\alpha\tilde{\omega} - \alpha\lambda|\omega_1|\tilde{\theta} \tag{11}$$

$$\dot{\tilde{\theta}} = \tilde{\omega} \tag{12}$$

which, in the derivative operator $p = d/dt$, has the characteristic polynomial $p^2 + \alpha p + \alpha\lambda|\omega_1|$. Assumed complex valued, the roots of this polynomial—i.e., the poles of the linearized system—are

$$p = -\frac{\alpha}{2} \pm j\sqrt{\alpha\lambda|\omega_1| - \left(\frac{\alpha}{2}\right)^2}. \tag{13}$$

For good damping of a system, the imaginary part of a conjugated pole pair should be equal to or smaller than the real part, moduluswise, which yields $\alpha \geq 2\lambda|\omega_1|$. To prevent that $\alpha = 0$ for $\omega_1 = 0$ (which, in turn, would prevent startup), the following selection rule is proposed

$$\alpha = \alpha_0 + 2\lambda|\omega_1| \tag{14}$$

where, as a rule of thumb, $\alpha_0 = 0.1\omega_{\rm base}$, with $\omega_{\rm base}$ being the base frequency. The poles then approach $p = \lambda|\omega_1|(-1 \pm j)$ asymptotically as ω_1 increases. Thus, for a constant λ, the estimator's convergence rate increases with the rotor speed.

B. Synchronization at Startup

Let us again assume accurate model motor parameters, and also, temporarily, assume that a "large" α is used, so that (9) can be considered in the steady state. Solving for ω_1 in the right-hand side of (9) then yields

$$\omega_1 = \omega_{\rm r}\cos\tilde{\theta} + \lambda_{\rm s}\omega_{\rm r}\sin\tilde{\theta}. \tag{15}$$

Notice that when $\tilde{\theta} = 0$, then $\omega_1 = \omega_{\rm r}$, as desired. By substituting (15) in (2), the position-error dynamics are obtained

$$\dot{\tilde{\theta}} = \omega_{\rm r}(1 - \cos\tilde{\theta}) - \lambda_{\rm s}\omega_{\rm r}\sin\tilde{\theta}. \tag{16}$$

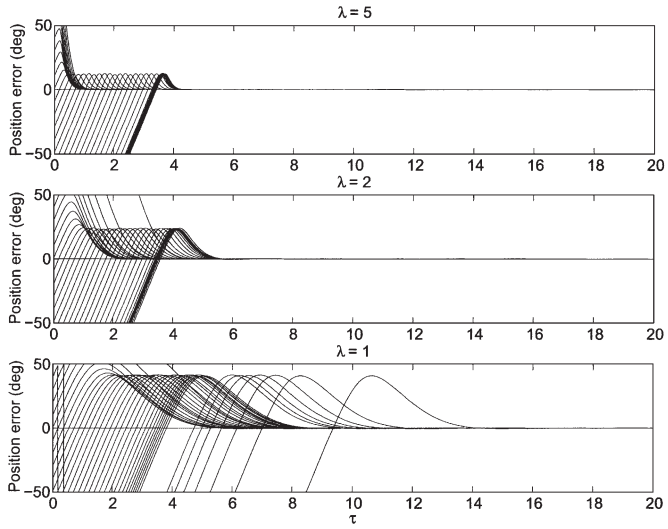

Fig. 2. Simulations for $\omega_{\rm r} > 0$ and three different choices of λ.

For a constant $\omega_{\rm r}$ (which in practice can be relaxed to a so-called quasi-constant $\omega_{\rm r}$; the estimator is assumed to converge much faster than the speed varies), an analytic solution exists

$$\cot\frac{\tilde{\theta}(t)}{2} = \frac{1}{\lambda_{\rm s}}\left[1 + \left(\lambda_{\rm s}\cot\frac{\tilde{\theta}(0)}{2} - 1\right)e^{\lambda_{\rm s}\omega_{\rm r}t}\right]. \tag{17}$$

For $\lambda_{\rm s}\omega_{\rm r} > 0$, i.e., $\mathrm{sgn}(\omega_1) = \mathrm{sgn}(\omega_{\rm r})$, the right-hand side of (17) tends to $\pm\infty$ as $t \to \infty$. Since $\lim_{x\to\pi}\cot nx = (-1)^n\infty$, n integer, it is clear that $\lim_{t\to\infty}\tilde{\theta}(t) = 2n\pi$, i.e., the desired convergence point.

However, when the motor starts rotating in the wrong direction [due to a large $\tilde{\theta}(0)$], the signs of $\omega_{\rm r}$ and ω_1 are different. It is important that the properties of the estimator are such that ω_1 then changes sign fairly quickly, for any $\tilde{\theta}(0)$. The discontinuous nonlinearity $\mathrm{sgn}(\omega_1)$ and the fact that α is not necessarily "large" when selected according to (14)—implying that the second-order systems (2) and (9) must be analyzed—make strict proof of convergence difficult. Therefore, we resort to simulating (2) and (9). By making repeated simulations for various initial values: $\tilde{\theta}(0) = n\Delta\theta$, $n = 1, 2, \ldots, 360^\circ/\Delta\theta$, for a small $\Delta\theta$, the convergence properties can be investigated for a certain value of λ, almost with the same rigor as in a theoretical analysis.

Since $\omega_{\rm r}$ acts as a gain parameter in (16), only its sign matters. A larger $\omega_{\rm r}$ merely implies faster convergence, not altered dynamic properties. Assuming—as for the analytic solution (17)—a quasi-constant $\omega_{\rm r}$, the system can be simulated in a normalized time scale: $\tau = |\omega_{\rm r}|t$. Fig. 2 shows simulations for $\omega_{\rm r} > 0$, three different gain parameter values: $\lambda = \{1, 2, 5\}$, and $\Delta\theta = 10^\circ$. Making $\omega_{\rm r} < 0$ produces, essentially, the vertical mirror image of Fig. 2. The following conclusions can be drawn as follows.

1) Synchronization is guaranteed; $\tilde{\theta}$ converges regardless of the initial position error, for all three choices of λ.
2) Making $\lambda < 2$ slows down the convergence noticeably, as seen by comparing the plots for $\lambda = 1$ and $\lambda = 2$.
3) Selecting $\lambda > 2$ has only a marginal impact, as seen by comparing the plots for $\lambda = 2$ and $\lambda = 5$.

Selecting $\lambda = 2$ (or slightly larger) is, therefore, a good recommendation. One should bear in mind that large gains also give a high amplification of noise [14].

C. Steady-State Position Error

Model motor parameter inaccuracies are now taken into account. Again solving for ω_1 in the right-hand side of (9) (observing that this time ω_1 appears in $\tilde{e}_d$ and $\tilde{e}_q$), and substituting the obtained expression in (2), yields

$$\dot{\tilde{\theta}} = \omega_{\rm r} - \frac{\tilde{R}_{\rm s}(i_q - \lambda_{\rm s} i_d) + \omega_{\rm r}\psi_{\rm m}(\cos\tilde{\theta} + \lambda_{\rm s}\sin\tilde{\theta})}{\hat{\psi}_{\rm m} - \tilde{L}_{\rm s}(i_d + \lambda_{\rm s} i_q)}. \quad (18)$$

From this relation, the steady-state position error can be found, by setting $\dot{\tilde{\theta}} = 0$. Under the simplifying assumption that the position error is small, such that $\cos\tilde{\theta} \approx 1$, we obtain by solving for $\sin\tilde{\theta}$

$$\sin\tilde{\theta}^{\star} = \frac{\tilde{R}_{\rm s}(\lambda_{\rm s} i_d - i_q)}{\lambda_{\rm s}\omega_{\rm r}\psi_{\rm m}} - \frac{\tilde{\psi}_{\rm m}}{\lambda_{\rm s}\psi_{\rm m}} - \frac{\tilde{L}_{\rm s}(i_d + \lambda_{\rm s} i_q)}{\lambda_{\rm s}\psi_{\rm m}} \quad (19)$$

where superscript "$\star$" indicates steady-state value (equilibrium point) and $\tilde{\psi}_{\rm m} = \psi_{\rm m} - \hat{\psi}_{\rm m}$. The following conclusions can be drawn.

1) At low speeds, the first term on the right-hand side of (19) dominates, due to its inverse proportionality to $\omega_{\rm r}$. Nonsalient PMSMs are, normally, operated with $i_d = 0$, giving $\sin\tilde{\theta}^{\star} \approx \tilde{R}_{\rm s} i_q/\lambda_{\rm s}\omega_{\rm r}\psi_{\rm m}$ for small $\omega_{\rm r}$. A large stator resistance error $\tilde{R}_{\rm s}$ and/or a large current i_q (i.e., high torque) dictates that a certain lowest operating speed must be observed, in order to keep the position error sufficiently small. Clearly, rotation reversal under load for $i_d = 0$ is difficult, unless the stator resistance is known with a very good accuracy.
2) If the stator current is controlled such that $i_d = i_q/\lambda_{\rm s}$ (instead of the usual $i_d = 0$), the sensitivity to $\tilde{R}_{\rm s}$ vanishes. Using a nonzero i_d to some extent reduces the current available for a torque production, since $i_d^2 + i_q^2 \leq I_{\rm max}^2$ where $I_{\rm max}$ is the maximum permissible current modulus. The following limitation is obtained

$$|i_q| \leq \frac{I_{\rm max}}{\sqrt{1 + \frac{1}{\lambda^2}}}. \quad (20)$$

   For a fairly large λ, the reduction in i_q is not significant. For example, $\lambda = 2$ yields $|i_q| \leq 0.89 I_{\rm max}$ while $\lambda = 3$ yields $|i_q| \leq 0.95 I_{\rm max}$. Controlling the stator current such that $i_d = i_q/\lambda_{\rm s}$ should, therefore, be the preferred strategy.
3) The parameter error $\tilde{\psi}_{\rm m}$ is normally small, due to a fairly constant magnet flux.
4) For fairly large λ, the position error due to the term $\tilde{L}_{\rm s} i_d/\lambda_{\rm s}\psi_{\rm m} = \tilde{L}_{\rm s} i_q/\lambda^2\psi_{\rm m}$ will be small.
5) Hence, the unavoidable position error, for $i_d = i_q/\lambda_{\rm s}$ with λ reasonably large ($\lambda \geq 2$), is given by

$$\sin\tilde{\theta}^{\star} \approx -\frac{\tilde{L}_{\rm s} i_q}{\psi_{\rm m}}. \quad (21)$$

Coincidentally, this is the same position error as for the estimator in [14].

Remark 1: Note that for a load torque that is constant or has constant sign, i_d will change sign at the moment of rotation reversal. Due to the well-known fact that i_d does not produce torque in a nonsalient PMSM under accurate field orientation conditions, using a nonzero i_d will not affect the operation of the motor in other ways than reducing $|i_q|$ according to (20). Making $i_d = i_q/\lambda_{\rm s}$ is, however, required only at low speeds, since the stator resistance is not a sensitive parameter at high speeds. Once out of the low-speed region (20%–30% of base speed should be sufficient), it is safe to let $i_d = 0$. Though $\hat{R}_{\rm s}$ then appears in the estimator equations, its impact is low, and a rough estimate (even $\hat{R}_{\rm s} = 0$) is sufficient.

Remark 2: Eliminating the sensitivity to the stator resistance is equivalent to using the instantaneous reactive power $q = v_d i_q - v_q i_d$ for estimation purposes [13], [15]. From (6), we have, with $\lambda_{\rm s} = i_q/i_d$

$$\omega_1 = \frac{e_q - \frac{i_q}{i_d} e_d}{\hat{\psi}_{\rm m}} = \frac{e_q i_d - e_d i_q}{\hat{\psi}_{\rm m} i_d} \quad (22)$$

in the steady state, where now q implicitly appears in the numerator, cf. (3).

Remark 3: In [16], it is shown that using $i_d \neq 0$ is beneficial also for a signal-injection-based sensorless control.

D. Prevention of Lockup at Low Speed

As discussed above in the Introduction, the problem of lockup at low speed for reversal of rotation is caused by the back EMF's proportionality to the speed. Examining (18), it is seen that if $i_d = i_q/\lambda_{\rm s}$, lockup may occur only at $\omega_{\rm r} = 0$, as the right-hand side then vanishes. This is not very critical, since $\omega_{\rm r} = 0$—standstill with applied stator current—by its very nature must be a marginally stable operating point. There can only be a temporary lockup.

For the sake of completeness, we also study operation with $i_d = 0$ (even at low speeds), should this for some reason be desired. The lockup speed is then, due to the term proportional to $\tilde{R}_{\rm s}$ in (18), moved from $\omega_{\rm r} = 0$ to a low speed, either positive or negative. This is much more serious, as this lockup may be permanent. An analysis is made in Appendix A, with the conclusion that if $\tilde{R}_{\rm s} > 0$ and $\tilde{L}_{\rm s} > 0$, the lockup speed will be positive for negative ω_1, and vice versa. This allows the rotation reversal to be completed without lockup, as when ω_1 changes sign, so does $\omega_{\rm r}^{\star}$. Simulations and experiments show that this does not eliminate the problem of limit cycles occurring for rotation reversal under load, however. In general, when $i_d = 0$, successful rotation reversals under load can only be accomplished if the stator resistance is accurately estimated ($\tilde{R}_{\rm s}/R_{\rm s}$ positive but small).

E. Stability and Dynamics for Closed-Loop Speed Control

Closing the speed-control loop for a sensorless drive implies that ω_1 is fed back and compared to the reference speed $\omega_{\rm ref}$ by a speed controller, whose output is (the reference for) i_q. Proportional-plus-integral (PI) controllers are the traditional

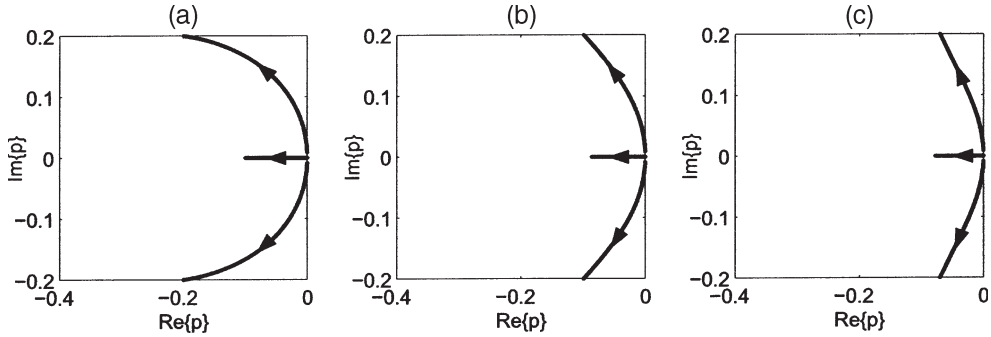

Fig. 3. Pole loci for $0 \leq \omega_{\rm ref} \leq 0.1$ pu and $\tilde{L}_{\rm s} = \{0.1, 0, -0.1\}$ pu: (a), (b), and (c), respectively.

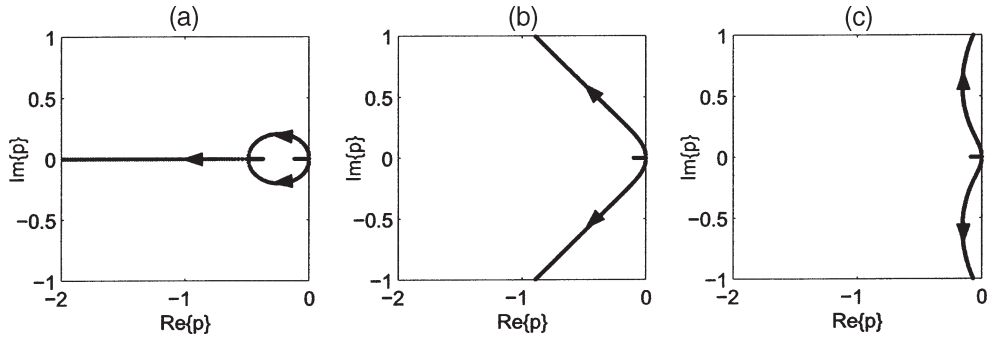

Fig. 4. Pole loci for $0 \leq \omega_{\rm ref} \leq 1$ pu and $\tilde{L}_{\rm s} = \{0.1, 0, -0.1\}$ pu: (a), (b), and (c), respectively.

speed controllers; a design method for a PI-type speed controller giving a bandwidth $\alpha_{\rm s}$ in the closed-loop system is presented in [17].

In Appendix B, it is shown analytically that the closed speed-control loop may turn unstable even for a moderately overestimated model stator inductance, if the speed-control loop is fast ($\alpha_{\rm s}$ large). Consequently, it is recommended that $\tilde{L}_{\rm s} > 0$ is ensured.

It is also enlightening to investigate the dynamics of the speed-control loop using numerical examples. The poles of the system (roots of the characteristic polynomial derived in Appendix B) are found numerically, for $\lambda = 2$, $a = 25$ pu, $\alpha_{\rm s} = 0.1$ pu (which is a fairly high bandwidth; see the next section), and a varying $\omega_{\rm ref}$. Pole loci are shown in Figs. 3 and 4. The following observations can be made.

1) The real-valued pole is due to the speed-control-loop dynamics. For sensorless control, the dynamics are by necessity poor at low speeds (due to the vanishing back EMF). Yet, the desired speed-control-loop dynamics, with a pole at $p \approx -\alpha_{\rm s} = -0.1$, are obtained already at $\omega_{\rm ref} = 0.1$ pu, as seen in Fig. 3.
2) An erroneous model stator inductance $\tilde{L}_{\rm s} \neq 0$ has only a marginal impact at low speeds.
3) For $\tilde{L}_{\rm s} = 0$—Fig. 4(b)—poles close to those desired, at $p = -\alpha_{\rm s}$ and $p = \lambda|\omega_1|(-1 \pm j)$, are obtained.
4) For $\tilde{L}_{\rm s} = 0.1$ pu, all three poles become real valued as $\omega_{\rm ref}$ increases, splitting the estimator dynamics into a slow and a fast mode (one pole much closer to the origin than the other). Yet, the "slow" pole is located farther from the origin than the pole at $p = -\alpha_{\rm s}$, and should, therefore, not have a major negative impact on the speed dynamics.
5) For $\tilde{L}_{\rm s} = -0.1$ pu, the system not surprisingly becomes poorly damped, with the complex-valued poles crossing into the right half-plane outside the area shown.

In conclusion, good dynamic performance except at very low speeds can be expected when the model stator inductance is underestimated.

IV. Experimental Evaluation

The purpose of this section is to verify the key properties of the estimator at low speeds, i.e., synchronization at startup and stable rotation reversal, especially under load. As the performance of the estimator at nominal speeds is verified in [11], only speeds below 0.1 pu are investigated. Data are as follows.

1) Motor: Manufacturer ELMO; 4.2 kW, six poles, connected to a dc-load machine. Base values: 195 V, 12 A, 1500 r/min, 16 Ω, 35 mH. Per-unit parameters: $L_{\rm s} = 0.27$, $R_{\rm s} = 0.03$, $\psi_{\rm m} = 1.0$, $J = 3500$.
2) Inverter: Manufacturer FRABIL; a 5.3-kHz switching frequency and a 540-V dc-link voltage are used.
3) Control: Texas Instruments TMS320C40 floating-point DSP, which uses a 5.3-kHz sampling frequency. Synchronous sampling of the stator currents is used in order to suppress switching harmonics, while rms-value space-vector scaling, $K = 1/\sqrt{2}$, is employed. The speed and current control loops (with PI-type controllers [17]) are tuned to give 10%–90% rise times of approximately 0.5 s

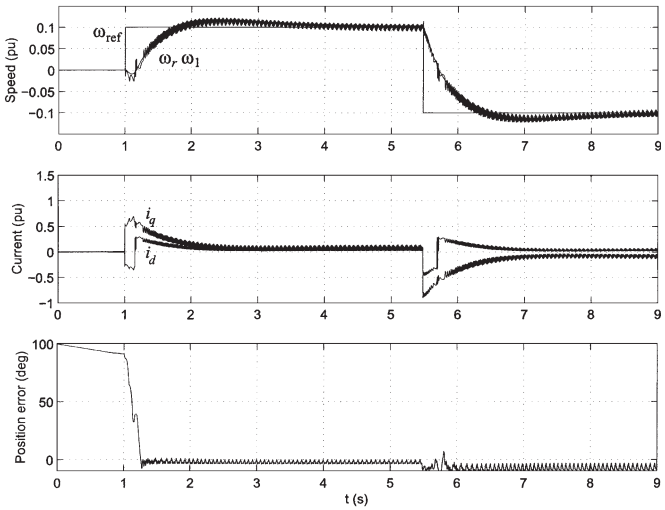

Fig. 5. Startup and positive-to-negative rotational reversal under no-load conditions.

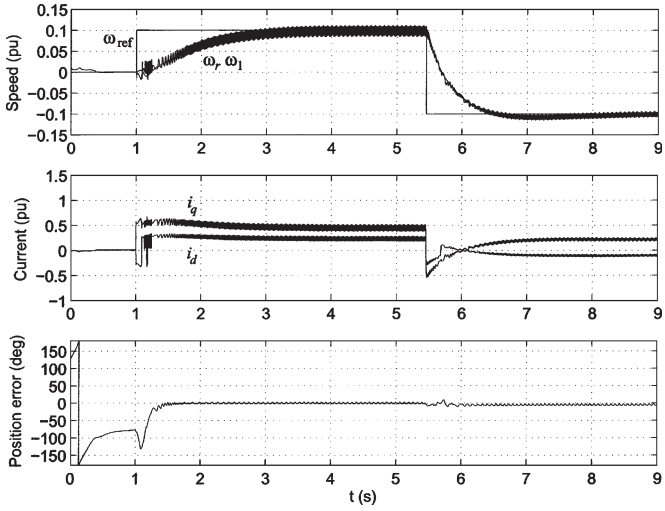

Fig. 6. Startup and positive-to-negative rotational reversal under load.

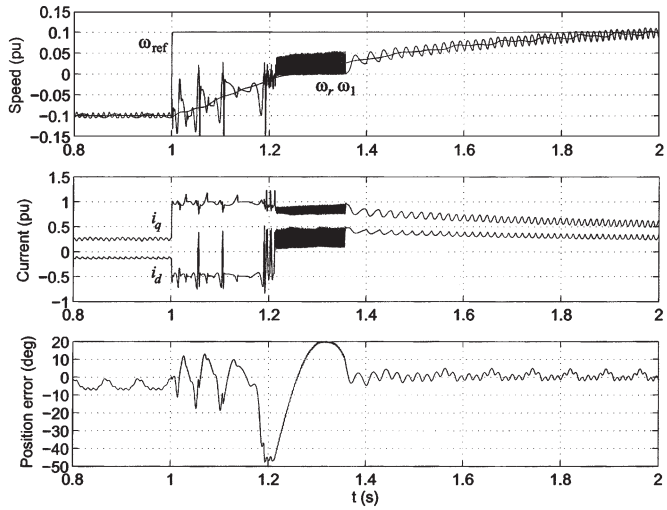

Fig. 7. Negative-to-positive rotational reversal under load.

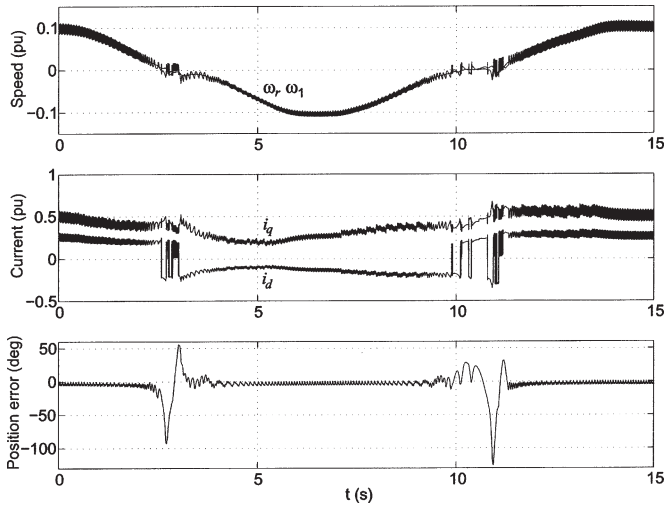

Fig. 8. Rampwise rotation reversals under load.

and 1.5 ms, respectively. Via the formula rise time $\times$ bandwidth $\approx \ln 9$, this yields $\alpha_s = 4.4$ rad/s $= 0.028$ pu (i.e., lower than the 0.1 pu used for Figs. 3 and 4) and, in turn, $k_p = 3.6$. In the position estimator, $\lambda = 2$ with $i_d = i_q/\lambda_s$ is used.

Successful startup and positive-to-negative rotational reversal are demonstrated in Figs. 5 and 6, under no-load conditions and with approximately half the rated load for positive speeds ($i_q = 0.5$ pu; created by applying an armature voltage in the dc-load machine), respectively. Notice the rapid convergence of the position error $\tilde{\theta}$ to a small value, even though the initial position error is large. Also notice the very small transient backward rotation: -0.01 pu only, and that the closed-loop speed dynamics are fast, with at most a small overshoot. Since the rotation reversal in Fig. 6 is made in the direction of the load torque, reversal is aided, giving hardly any transient deviation from the small steady-state position error. It should finally be noted that the mean steady-state position error is slightly larger for negative speeds than for positive. This is in agreement with (19), which predicts a position error that, via λ_s, is dependent on the sign of the speed, also when $i_d = i_q/\lambda_s$.

In Fig. 7, a more difficult negative-to-positive rotation reversal against the load torque (which demands a torque-producing current component of 1 and 0.6 pu at the transient and in the steady state, respectively) is depicted. While a larger transient position error here results—which is likely due to slower speed-control-loop dynamics at very low speeds—synchronism is maintained, and the reversal is successfully completed.

In Fig. 8, the reference speed changes ramp wise from $0.1-0.1$ pu and vice versa; each reversal taking 6 s. As in Fig. 7, a large transient position error appears at the moment the rotation reverses, but synchronism is kept and both reversals are completed successfully.

Remark 4: While the noise (ripple) in ω_1 is fairly large, especially in Fig. 7, the noise level will not increase with the speed, due to a constant gain λ. Rather, the relative noise level will decrease. Note also that the actual speed is smooth, which can be clearly seen in Fig. 7.

V. Conclusion

The proposed estimator, called the "statically compensated voltage model," was in theory, simulations, and experiments found to give synchronization at startup, even after an initial rotation in the wrong direction, as well as a stable reversal of rotation under load. The desired dynamics of the speed-control loop (with bandwidth $\alpha_{\rm s}$) were shown to be obtained, except at very low speeds. The requirements are as follows.

1) At low speeds, the stator current must be controlled such that $i_d = i_q \mathrm{sgn}(\omega_1)/\lambda$, with $2 \leq \lambda \leq 3$ being the recommendation for this gain parameter. This implies using the instantaneous reactive power for estimation purposes, which removes sensitivity to the stator resistance. The position error is, thus, kept small (except at the moment of rotation reversal).
2) The stator inductance should be underestimated: $\hat{L}_{\rm s} < L_{\rm s}$, in order to guarantee stability of the closed speed-control loop.

If, for some reason, it is desired that $i_d = 0$, the following recommendations should be followed.

1) Also, the stator resistance should be underestimated: $\hat{R}_{\rm s} < R_{\rm s}$. If not, lockup may occur at a low speed when rotation reversal is attempted. Found empirically in [11], this result was here verified analytically.
2) Unless $\hat{R}_{\rm s}$ is very accurately estimated, rotation reversal should only be attempted when the load is light, as the position error otherwise will become very large for low speeds, giving loss of torque. This prevents reversal, giving instead limit-cycle oscillations about a low speed.

Future research should focus on methods for reducing the transient error at rotation reversal, and also reducing the noise content of the speed estimate.

Finally, as the estimator, with minor modifications, can be used for sensorless control also of induction motors [11], it is worth pointing out that the strategy of selecting $i_d = i_q \mathrm{sgn}(\omega_1)/\lambda$ then cannot be used, since i_d controls the flux and is not available for manipulation. For an induction motor, reactive power approaches do not give a stable system when the speed and torque have different signs [13].

Appendix A
Prevention of Lockup for $i_d = 0$

The lockup position $\tilde{\theta}^\star$ can be found using the mechanical dynamics

$$\frac{J}{n_p}\dot{\omega}_{\rm r} = k(i_q \cos\tilde{\theta} - i_d \sin\tilde{\theta}) - \tau_{\rm L} \tag{23}$$

where J is the inertia, n_p is the number of pole pairs, $\tau_{\rm L}$ is the load torque, and $k = 3n_p\psi_{\rm m}/2K^2$ where K is the space-vector scaling constant. For $i_d = 0$ and a light load, $\tau_{\rm L} \approx 0$, but yet a fairly large i_q in order to produce enough torque for the rotation reversal, it is seen that *if* the speed locks up, such that $\dot{\omega}_{\rm r} = 0$, then the position must lock up at an error $\tilde{\theta}^\star$ close to $90^\circ \mathrm{sgn}(i_q)$. As the load torque increases, $\tilde{\theta}^\star$ will decrease, but not change sign, as long as $\tau_{\rm L}$ has the same sign as i_q, so

$$\tilde{\theta}^\star = \mathrm{sgn}(i_q)\vartheta, \qquad 0 < \vartheta < 90^\circ. \tag{24}$$

For simplicity, let us assume that $\hat{\psi}_{\rm m} = \psi_{\rm m}$ in (18). Putting $\tilde{\theta} = 0$ and solving for $\omega_{\rm r}$ then yields the following expression for the lockup speed, with $\tilde{\theta} = \mathrm{sgn}(i_q)\vartheta$

$$\begin{aligned} \omega_{\rm r}^\star &= \frac{\tilde{R}_{\rm s} i_q}{\psi_{\rm m} D(\vartheta)} \\ D(\vartheta) &= 1 - \frac{\lambda_{\rm s}\tilde{L}_{\rm s} i_q}{\psi_{\rm m}} - \cos\vartheta - \lambda_{\rm s}\mathrm{sgn}(i_q)\sin\vartheta. \end{aligned} \tag{25}$$

It is easily verified that for $0 < \vartheta < 90^\circ$ and $\tilde{L}_{\rm s} \geq 0$, $D(\vartheta)$ has the opposite sign to $\mathrm{sgn}(\omega_1)\mathrm{sgn}(i_q)$, for any $\lambda > 1$. Thus, we find that

$$\omega_{\rm r}^\star \sim -\tilde{R}_{\rm s} i_q \mathrm{sgn}(\omega_1)\mathrm{sgn}(i_q) = -\tilde{R}_{\rm s}|i_q|\mathrm{sgn}(\omega_1) \tag{26}$$

where "$\sim$" stands for "proportional to." Therefore, by underestimating both the stator resistance and the stator inductance: $\tilde{R}_{\rm s} > 0$, $\tilde{L}_{\rm s} > 0$, the lockup speed will be positive for negative ω_1, and vice versa.

Appendix B
Analysis of the Closed Speed-Control Loop

Let us for simplicity disregard the integral part of the PI speed controller, letting $i_q = k_p(\omega_{\rm ref} - \omega_1)$. With $p = d/dt$, $\omega_1 = \omega_{\rm r}$, and $\tilde{\theta} = \tau_{\rm L} = 0$, the mechanical dynamics (23) can then be expressed as

$$\omega_{\rm r} = \frac{1}{p}\frac{k_p n_p k}{J}(\omega_{\rm ref} - \omega_{\rm r}) \Rightarrow \omega_{\rm r} = \frac{\alpha_{\rm s}}{p + \alpha_{\rm s}}\omega_{\rm ref} \tag{27}$$

for $k_p = \alpha_{\rm s} J/kn_p$. However, $\omega_1 = \omega_{\rm r}$ cannot immediately be assumed for a sensorless drive; the position estimator must be taken into account when analyzing the speed-control loop. Assuming a small $\tilde{\theta}$, $\hat{\psi}_{\rm m} = \psi_{\rm m}$, and $i_d = i_q/\lambda_{\rm s}$, (9) yields

$$\frac{e_q - \lambda_{\rm s} e_d}{\hat{\psi}_{\rm m}} = \left(\lambda + \frac{1}{\lambda}\right)\frac{|\omega_1|\tilde{L}_{\rm s} i_q}{\psi_{\rm m}} + \omega_{\rm r} + \lambda_{\rm s}\omega_{\rm r}\tilde{\theta} - \omega_1. \tag{28}$$

Error variables $\tilde{\omega} = \omega_{\rm r} - \omega_1$ and $\varepsilon = \omega_{\rm ref} - \omega_1$ are introduced, giving $i_q = k_p\varepsilon = (\alpha_{\rm s} J/kn_p)\varepsilon$. We also introduce the following parameter

$$a = \left(\lambda + \frac{1}{\lambda}\right)\frac{\alpha_{\rm s} J}{kn_p\psi_{\rm m}} = \left(\lambda + \frac{1}{\lambda}\right)\frac{k_p}{\psi_{\rm m}}. \tag{29}$$

Then, with $\alpha \approx 2\lambda|\omega_1|$, (28) substituted in (6) yields

$$\dot{\omega}_1 = 2\lambda|\omega_1|\left(a|\omega_1|\tilde{L}_{\rm s}\varepsilon + \tilde{\omega} + \lambda_{\rm s}\omega_{\rm r}\tilde{\theta}\right) = -\dot{\varepsilon} \tag{30}$$

where for the second equality, a constant $\omega_{\rm ref}$ is assumed. With $\tau_{\rm L}=0$ and $i_q=(\alpha_{\rm s}J/kn_p)\varepsilon$, the mechanical dynamics (23) can be expressed as

$$\dot{\omega}_{\rm r}=\alpha_{\rm s}\varepsilon\left(1-\frac{1}{\lambda_{\rm s}}\tilde{\theta}\right)=\dot{\tilde{\omega}}-\dot{\varepsilon}. \tag{31}$$

Linearizing (30) and (31) about $\omega_{\rm r}=\omega_1=\omega_{\rm ref}$, while approximating $\tilde{\theta}\approx 0$ in (31), together with (2) the following third-order system is obtained

$$\dot{\varepsilon}=-2\lambda|\omega_{\rm ref}|\left(a|\omega_{\rm ref}|\tilde{L}_{\rm s}\varepsilon+\tilde{\omega}+\lambda|\omega_{\rm ref}|\tilde{\theta}\right) \tag{32}$$

$$\dot{\tilde{\omega}}=\alpha_{\rm s}\varepsilon-2\lambda|\omega_{\rm ref}|\left(a|\omega_{\rm ref}|\tilde{L}_{\rm s}\varepsilon+\tilde{\omega}+\lambda|\omega_{\rm ref}|\tilde{\theta}\right) \tag{33}$$

$$\dot{\tilde{\theta}}=\tilde{\omega} \tag{34}$$

which has the characteristic polynomial $p^3+a_2p^2+a_1p+a_0$, where

$$a_2=2\lambda|\omega_{\rm ref}|\left(1+a|\omega_{\rm ref}|\tilde{L}_{\rm s}\right) \tag{35}$$

$$a_1=2\lambda|\omega_{\rm ref}|\left(\alpha_{\rm s}+\lambda|\omega_{\rm ref}|\right) \tag{36}$$

$$a_0=2\alpha_{\rm s}(\lambda\omega_{\rm ref})^2. \tag{37}$$

Asymptotic stability of a third-order system requires that $\{a_0,a_1,a_2\}>0$ and, according to Routh's test, also that

$$a_1a_2-a_0=2(\lambda\omega_{\rm ref})^2\left\{\alpha_{\rm s}+2|\omega_{\rm ref}|\left[\lambda+a(\lambda|\omega_{\rm ref}|+\alpha_{\rm s})\tilde{L}_{\rm s}\right]\right\}>0. \tag{38}$$

Stability is guaranteed for $\tilde{L}_{\rm s}\geq 0$, i.e., an underestimated model stator inductance. Let us determine whether there is a risk for instability for reasonable $\tilde{L}_{\rm s}<0$. To achieve $a_2>0$, it is required that $\tilde{L}_{\rm s}>-1/a|\omega_{\rm ref}|$, while (38) yields

$$\tilde{L}_{\rm s}>-\frac{1}{a|\omega_{\rm ref}|}\underbrace{\frac{1+\frac{\alpha_{\rm s}}{2\lambda|\omega_{\rm ref}|}}{1+\frac{\alpha_{\rm s}}{\lambda|\omega_{\rm ref}|}}}_{q} \tag{39}$$

which, since $1/2<q<1$, is the more strict condition. To give a numerical example, for the parameters in Section IV, we obtain $\tilde{L}_{\rm s}>-0.11$ pu, i.e., overestimation of $L_{\rm s}$ by 41% is allowed. Though this may seem generous, the tolerance will shrink for drives with faster speed-control loops, so it is always recommended to use $\hat{L}_{\rm s}<L_{\rm s}$.

APPENDIX C
SAMPLE C-CODE IMPLEMENTATION

The code below exemplifies how the estimator can be implemented using forward difference discretization (with sampling period `T`) as a few lines of code in the programming language C. `WLIM` is the frequency (0.2 to 0.3 pu) below which the selection $i_d^{\rm ref}=i_q^{\rm ref}/\lambda_{\rm s}$ should be used, while `fsgn` is assumed to be a function which takes the sign of its floating-point argument. All other variables and constants should be readily identifiable from the notation used in the paper.

```
if (fabs(w1) > WLIM) idref = 0;
  else idref = iqref/LAMBDA * fsgn(w1);
current_controller(&vdref, &vqref,
  &idref, &iqref, theta);
ed = vdref - RSH * idref + w1 * LSH * iqref;
eq = vqref - RSH * iqref - w1 * LSH * idref;
alpha = ALPHA0 + 2 * LAMBDA * fabs(w1);
w1 += T * alpha * (
  (eq-LAMBDA * fsgn(w1) * ed)/PSIMH - w1);
theta += T * w1;
while (theta > PI) theta -= 2 * PI;
while (theta <- PI) theta += 2 * PI;
```

REFERENCES

[1] M. Schroedl, "Sensorless control of permanent magnet synchronous motors," *Electr. Mach. Power Syst.*, vol. 22, no. 2, pp. 173–185, Mar./Apr. 1994.

[2] M. J. Corley and R. D. Lorenz, "Rotor position and velocity estimation for a salient-pole permanent magnet synchronous machine at standstill and high speeds," *IEEE Trans. Ind. Appl.*, vol. 34, no. 4, pp. 784–789, Jul./Aug. 1998.

[3] C. Silva, G. M. Asher, M. Sumner, and K. J. Bradley, "Sensorless rotor position control in a surface mounted PM machine using HF rotating injection," *EPE J.*, vol. 13, no. 3, pp. 12–17, Aug. 2003.

[4] J.-H. Jang, S.-K. Sul, J.-I. Ha, K. Ide, and M. Sawamura, "Sensorless drive of surface-mounted permanent-magnet motor by high-frequency signal injection based on magnetic saliency," *IEEE Trans. Ind. Appl.*, vol. 39, no. 4, pp. 1031–1039, Jul./Aug. 2003.

[5] L. Harnefors, "On analysis, control and estimation of variable-speed drives," Ph.D. dissertation, Electrical Machines and Drives, Dept. Electr. Power Eng., Royal Inst. Technol., Stockholm, Sweden, 1997.

[6] B. Nahid Mobarakeh, F. Meibody-Tabar, and F. M. Sargos, "A globally converging observer of mechanical variables for sensorless PMSM," in *Proc. IEEE Power Electron. Specialists Conf.*, vol. 2, pp. 885–890.

[7] N. Matsui, "Sensorless PM brushless DC motor drives," *IEEE Trans. Ind. Electron.*, vol. 43, no. 2, pp. 300–308, Apr. 1996.

[8] S. Bolognani, R. Oboe, and M. Zigliotto, "Sensorless full-digital PMSM drive with EKF estimation of speed and rotor position," *IEEE Trans. Ind. Electron.*, vol. 46, no. 1, pp. 184–191, Feb. 1999.

[9] K. Tatematsu, D. Hamada, K. Uchida, S. Wakao, and T. Onuki, "New approaches with sensorless drives," *IEEE Ind. Appl. Mag.*, vol. 6, no. 4, pp. 44–50, Jul./Aug. 2000.

[10] L. Ying and N. Ertugrul, "A novel, robust DSP-based indirect rotor position estimation for permanent magnet AC motors without rotor saliency," *IEEE Trans. Power Electron.*, vol. 18, no. 2, pp. 539–546, Mar. 2003.

[11] L. Harnefors, M. Jansson, R. Ottersten, and K. Pietiläinen, "Unified sensorless vector control of synchronous and induction motors," *IEEE Trans. Ind. Electron.*, vol. 50, no. 1, pp. 153–160, Feb. 2003.

[12] M. Jansson, L. Harnefors, and K. Pietiläinen, "Guaranteed synchronization of non-salient PMSM drives," in *Proc. Eur. Conf. Power Electron. and Applications*, Toulouse, France, Sep. 2003, CD-ROM.

[13] L. Harnefors, "Design and analysis of general rotor-flux-oriented vector control systems," *IEEE Trans. Ind. Electron.*, vol. 48, no. 2, pp. 383–390, Apr. 2001.

[14] L. Harnefors and H.-P. Nee, "A general algorithm for speed and position estimation of AC motors," *IEEE Trans. Ind. Electron.*, vol. 47, no. 1, pp. 77–83, Feb. 2000.

[15] F.-Z. Peng and T. Fukao, "Robust speed identification for speed-sensorless vector control of induction motors," *IEEE Trans. Ind. Appl.*, vol. 30, no. 5, pp. 1234–1240, Sep./Oct. 1994.

[16] E. Robeischl and M. Schroedl, "Direct axis current utilization for intelligent sensorless permanent magnet synchronous drives," in *Proc. Conf. Rec. IEEE 36th IAS Annu. Meeting*, Sep./Oct. 2001, vol. 1, pp. 475–481.

[17] L. Harnefors, K. Pietiläinen, and L. Gertmar, "Torque-maximizing field-weakening control: Design, analysis, and parameter selection," *IEEE Trans. Ind. Electron.*, vol. 48, no. 1, pp. 161–168, Feb. 2001.

Magnus Jansson was born in 1973 in Eskilstuna, Sweden. He received the M.Sc. degree in electrical engineering from Mälardalen University, Västerås, Sweden, in 1999, where he successfully defended his Ph.D. dissertation in 2005.

Between 1999 and 2004, he was with the Department of Electronics, Mälardalen University, as a Research Assistant. He is now with ABB Automation Products, Västerås. His research interests include control of variable-speed drives and electrical machine design.

Lennart Harnefors (S'93–M'97) was born in 1968 in Eskilstuna, Sweden. He received the M.Sc., Licentiate, and Ph.D. degrees in electrical engineering from the Royal Institute of Technology, Stockholm, Sweden, and the Docent (D.Sc.) degree in industrial automation from Lund University, Lund, Sweden, in 1993, 1995, 1997, and 2000, respectively.

From 1994 to 2005, he was with Mälardalen University, Västerås, Sweden, where he, in 2001, was appointed Professor of Electrical Engineering. He is now with ABB Power Systems, Ludvika, Sweden. Since 2001, he has also been a Part-Time Visiting Professor of Electrical Drives at Chalmers University of Technology, Göteborg, Sweden. His research interests include applied signal processing and control, in particular, control of power electronic systems and ac drives.

Dr. Harnefors was the recipient of the 2000 ABB Gunnar Engström Energy Award and the 2002 IEEE TRANSACTIONS ON INDUSTRIAL ELECTRONICS Best Paper Award. He is an Associate Editor of the IEEE TRANSACTIONS ON INDUSTRIAL ELECTRONICS.

Oskar Wallmark (S'01) was born in 1976 in Falun, Sweden. He received the M.Sc. degree in engineering physics and the Licentiate degree in electrical engineering from Chalmers University of Technology, Göteborg, Sweden, in 2001 and 2004, respectively, where he is currently working toward the Ph.D. degree in the Department of Energy and Environment.

His research interests include control of electrical drives, particularly in hybrid and electric vehicle applications.

Mats Leksell (S'91–M'99) was born in 1957 in Stockholm, Sweden. He received the M.Sc. and Licentiate degrees in electrical engineering from the Royal Institute of Technology, Stockholm, Sweden, in 1984 and 1992, respectively.

Since 1992, he has been a Research Engineer at the Royal Institute of Technology, currently with the School of Electrical Engineering. His interests are power electronics, variable-speed drives, and electrical machine design.